2016

Hydraulic Conductivity as a Proxy for Drainage System Connectivity in a Subglacial Hydrology Model

Jacob Z. Downs
University of Montana, Missoula

HYDRAULIC CONDUCTIVITY AS A PROXY FOR DRAINAGE SYSTEM CONNECTIVITY IN A SUBGLACIAL HYDROLOGY MODEL

By

JACOB Z. DOWNS

B.S. Computer Science, Rocky Mountain College, Missoula, MT, 2013
B.S. Mathematics, Rocky Mountain College, Missoula, MT, 2013

Thesis

presented in partial fulfillment of the requirements for the degree of

Master of Science
in Computer Science

The University of Montana
Missoula, MT

December 2016

Approved by:

Scott Whittenburg, Dean of The Graduate School
Graduate School

Dr. Jesse V. Johnson, Chair
Computer Science

Dr. Joel T. Harper
Geosciences

Dr. Rob Smith
Computer Science

Downs, Jacob, M.S., Fall 2016 **Computer Science**

Hydraulic conductivity as a proxy for drainage system connectivity in a subglacial hydrology model

Committee Chair: Jesse V. Johnson

ABSTRACT
The link between subglacial hydrology and basal sliding has prompted work on basal hydrology models with water pressure and storage as prognostic variables. We find that a commonly used model of distributed drainage through linked cavities underpredicts winter water pressure when compared to borehole observations from Isunnguata Sermia in Western Central Greenland. Possible causes for this discrepancy including unrealistic model inputs or unconstrained parameters are investigated through a series of modeling experiments on both synthetic and realistic ice sheet geometries. We find that conductivity acts as a proxy for the connectivity of the linked cavity system and should therefore change seasonally. Model experiments also suggest that trends in winter sliding velocity are more closely related to winter water storage rather than pressure.

ACKNOWLEDGMENTS

My sincere thanks to:

- Jesse Johnson, Joel Harper, and Toby Meierbachtol for helping to set a direction for this project and suffering through lots of my writing. Your input has helped to significantly improve the organization and clarity of this thesis.
- Jesse in particular for his support, guidance, and patience over the past few years. I'm glad you took a chance on me based on some silly data viz. projects featuring strange loops in classical music or Lovecraftian aliens in Antarctica.
- Everyone who has worked so hard in the field including Joel, Toby, Kaitlyn, Ben, and Patrick. Without their efforts this thesis would not have been possible.
- The fine people I work alongside (or perpendicular to, considering the orientation of my desk) for chats that help break up the work day (and also for not laughing at my stupid questions).
- Kaitlyn for some good philosophical conversations.
- Evan for helping me work through many a FEniCS quandary.
- My family for their love and support.
- Mauro Werder and Christian Schoof for kindly taking time to answer some of my modeling related questions.
- The NSF for supporting this work through grant number 1543533.

TABLE OF CONTENTS

		Page
1.1	Introduction	1
1.2	Model Description	3
	1.2.1 Numerical Solution	9
	1.2.2 Model Limitations	9
1.3	Synthetic Experiments and Results	10
	1.3.1 Reference Experiment (REF)	11
	1.3.2 Sliding and Bump Parameter Experiment (SBP)	13
	1.3.3 Time Varying Conductivity and Sliding	16
1.4	Realistic Experiments and Results	20
	1.4.1 Reference Experiment on Realistic Geometry (REFR)	21
	1.4.2 Time Variable Sliding on Realistic Geometry (TVSR)	22
	1.4.3 Time Dependent Sliding and Conductivity on Realistic Geometry (TDSCR)	23
1.5	Discussion	26
	1.5.1 Physical Motivation for Changing Conductivity	26
	1.5.2 Constraining Conductivity	27
	1.5.3 Implications for Sliding	29
	1.5.4 Conclusions and Future Work	30
1.6	Code Repository	31

Hydraulic Conductivity as a Proxy for Drainage System Connectivity in a Subglacial Hydrology Model

Preface

This thesis has been written in journal article format intended for submission for publication in 2016.

1.1 Introduction

Surface melt input into the subglacial drainage system plays a significant role in controlling the rate of basal sliding of the Greenland Ice Sheet [*Shepherd et al.*, 2009, *van de Wal et al.*, 2008, *Zwally et al.*, 2002]. Surface melt is known to enhance ice flow as surface velocities can more than double from winter to early summer [*Bartholomew et al.*, 2010, *Sundal et al.*, 2011]. However, relationship between surface melt and basal sliding is poorly understood. More surface melt does not necessarily translate to faster basal sliding. The complex coupling between surface melt and sliding speed depends on the evolution of the subglacial drainage system as it adapts to variations in melt input to the bed on diurnal and seasonal time scales [*Hewitt et al.*, 2012].

Seminal publications such as *Budd et al.* [1979] and *Bindschadler* [1979] have long recognized a possible link between water pressure in the subglacial drainage system and basal sliding. Efforts are ongoing to develop sliding laws that mathematically relate sliding velocity to water pressure [e.g. *Schoof*, 2005]. Sliding laws formalize the intuitive idea that higher water pressure reduces contact between the ice sheet and bed leading to faster sliding. Borehole pressure measurements in Greenland illustrate a shortcoming of this idea. Measurements presented in *Wright et al.* [2016], *Ryser et*

al. [2014], and *Meierbachtol et al.* [2013] show that borehole pressures remain high through the fall and winter even as sliding speed decreases.

The difficulty of directly observing the subgacial drainage system has motivated work on basal hydrology models capable of capturing the evolution of the drainage system by simulating water storage and pressure. Models of distributed drainage through linked cavities introduced by *Hewitt* [2011] and *Schoof et al.* [2012] have provided a versatile foundation for a family of recent models that incorporate additional drainage elements such as channels [*Hewitt et al.*, 2012, *Werder et al.*, 2013] and till [*Bueler and van Pelt*, 2014]. Model developers face the difficult task of balancing practical mathematical and computational concerns with physical fidelity. Decisions about what drainage elements to include or whether certain simplifications to the physics are justified must be weighed against sparse observations.

A known problem with current models is their tendency to underpredict winter water pressure [*Flowers*, 2015]. The inability of models to predict high winter pressure suggests they may be neglecting or oversimplifying an important physical process. Previous modeling work has focussed on the evolution of the drainage system during the melt season, but the winter mode of the drainage system is perhaps equally important. *Sole et al.* [2013] have observed that high melt years do not have significantly faster surface velocities than low melt years because fast summer ice flow is offset by slow ice flow in subsequent winters. The winter dynamics of the subglacial drainage system are important for determining total annual ice flow.

Here we address the problem of low modeled winter water pressure. We find that a commonly used subglacial hydrology model posed by *Schoof et al.* [2012] severely underpredicts winter water pressure when compared to borehole observations. Through a gamut of simulations on both synthetic (section **??**) and realistic (section **??**) ice sheet geometries, we investigate a number of possible causes of low modeled pressure including unrealistic model input and poorly constrained parameters.

We conclude that the hydraulic conductivity parameter in *Schoof et al.* [2012] and related models, which is usually treated as a constant, serves as a proxy for

the connectivity of the linked cavity system and should therefore undergo seasonal changes (section 1.5). Our results allude to significant variations in the efficiency of the distributed drainage system as hypothesized by *Meierbachtol et al.* [2013] and *Andrews et al.* [2014]. Results also indicate that there may be less winter water storage after high melt summers than low melt summers, providing an alternative explanation for trends in winter sliding speed observed by *Sole et al.* [2013].

1.2 Model Description

We implement a model of distributed drainage through linked cavities developed by *Schoof et al.* [2012]. The model predicts spatially averaged sheet height h and hydraulic potential ϕ on a two-dimensional spatial domain Ω with boundary $\partial\Omega$. Model inputs include bed elevation B, ice thickness H, melt input to the bed m, and sliding speed u_b. *Schoof et al.* [2012] arrive at their continuum description of flow through linked cavities by starting with an ODE for cross sectional area S of a single cavity. S undergoes a spatial averaging process to arrive at a new ODE for spatially averaged cavity height h (sometimes also referred to as sheet height or sheet thickness). Physically, h is the average height of all discrete cavities and links over an area determined by the the spatial resolution of the computational mesh used in simulations. *Schoof et al.* [2012] make the simplifying assumption that links between cavities are controlled by the same balance of opening and closing processes as cavities and that their size therefore scales with cavity size.

Cavity height h is modelled as a balance between opening v_o due to sliding over bedrock bumps and creep closure v_c:

$$\frac{\partial h}{\partial t} = v_o(h) - v_c(N,h) = \frac{u_b(h_r - h)}{l_r} - AhN^3 \tag{1.1}$$

Here h_r is characteristic bump height, l_r is characteristic bump length, A is the rate factor for ice, and N is effective pressure. Cavity opening due to melting of cavity walls is assumed to be negligible. Effective pressure is defined as

$$N = p_i - p_w$$

where $p_i = \rho_i g H$ is ice overburden pressure and p_w is the water pressure. Hydraulic potential ϕ and water pressure are directly related. In particular

$$\phi = \phi_m + p_w$$

where $\phi_m = \rho_w g B$ is the elevation potential. Hence, effective pressure can also be related directly to the primary model unknown ϕ by

$$N = \phi_0 - \phi$$

with $\phi_0 = \phi_m + p_i$.

The height of water h_w within cavities obeys a conservation equation

$$\frac{\partial h_w}{\partial t} + \nabla \cdot \mathbf{q} = m \tag{1.2}$$

with melt input to the bed m and flux $\mathbf{q}$. *Schoof et al.* [2012] propose a general spatially averaged flux relation of the form:

$$\mathbf{q} = -k h_w^{\alpha} |\nabla \phi|^{\beta - 2} \nabla \phi \tag{1.3}$$

Here k is hydraulic conductivity, $\alpha \geq 1$, and $\beta > 1$. We use $\alpha = \frac{5}{4}$ and $\beta = \frac{3}{2}$ for turbulent flow. Broadly speaking, k affects how easily water flows through the drainage system. It is useful to motivate the role of k by considering the case when

Table 1.1: This table summarizes all model constants, inputs, and parameters. Default values are provided where applicable.

Description	**Symbol**	**Value**	**Units**
Constants			
Gravitational acceleration	g	9.81	m s^{-2}
Ice density	ρ_i	910	kg m^{-3}
Water density	ρ_w	1000	kg m^{-3}
Rate factor for ice	A	5×10^{-25}	Pa^{-3} s^{-1}
Flux exponent	α	5/4	-
Flux exponent	β	3/2	-
Model Inputs			
Bed elevation	B	-	m
Ice thickness	H	-	m
Melt input	m		m s^{-1}
Sliding speed	u_b	-	m s^{-1}
Potential at 0 pressure	ϕ_m	$\rho_w g B$	Pa
Ice overburden pressure	p_i	$\rho_i g H$	Pa
Overburden Potential	ϕ_0	$\phi_m + p_i$	Pa
Model Outputs			
Cavity height	h	-	m
Hydraulic potential	ϕ	-	Pa
Water Pressure	p_w	$\phi - \phi_m$	Pa
Effective Pressure	N	$\phi_0 - \phi$	Pa
Model Parameters			
Hydraulic Conductivity	k	-	$m^{7/4} kg^{-1/2}$
Bump height	h_r	0.1	m
Bump spacing	l_r	2	m

$\beta = 2$ and $\alpha = 1$ in which (1.3) simplifies to Darcy's law for flow through a porous medium

$$\mathbf{q} = -kh_w \nabla \phi.$$

In Darcy's law, hydraulic conductivity can be written as $k = k_0/\eta$ where k_0 is the intrinsic permeability of the porous medium and η is the viscosity of the fluid. Increasing fluid viscosity or decreasing permeability reduces the conductivity, thereby increasing flow resistance. In the more general context of equation (1.3), k may depend on the geometry of the local drainage system. *Clarke* [1996] presents a flux relation for laminar flow through parallel sided plates

$$\mathbf{q} = -\frac{w}{12\eta l} h_w^3 \nabla \phi$$

where w is the cross-flow width of the sheet and l is the along flow length. *Hewitt* [2011] writes this flux relation in a form resembling Darcy's law:

$$\mathbf{q} = -\frac{k_0}{\eta} h_w^3 \nabla \phi = -k h_w^3 \nabla \phi$$

Here, $k_0 = w/12l$ is now a geometric factor. We can think of $k = k_0/\eta$ as analagous to the hydraulic conductivity familiar from Darcy's law, bearing in mind that its precise physical meaning is now different as it depends on drainage system geometry rather than the permeability of some porous medium.

Similarly *Bueler and van Pelt* [2014] write the turbulent flux relation (1.3) with $\alpha = \frac{5}{4}$ and $\beta = \frac{3}{2}$ in the style of Darcy's law

$$\mathbf{q} = -K h_w \nabla \phi.$$

where $K = k h_w^{\alpha-1} |\nabla \phi|^{\beta-2}$ is called the effective conductivity. *Clarke* [1996] notes that for turbulent flow through conduits, effective conductivity depends on the local drainage system geometry, a roughness measure, as well as the hydraulic potential.

In the present case, we interpret the term $kh_w^{\alpha-1}$ as a primarily geometric factor that depends on the subgrid scale drainage system geometry as well as bed roughness.

Between equations (1.1) and (1.2) there are three unknowns (h, h_w, and ϕ). To close the model, *Schoof et al.* [2012] assume that cavities are initially fully saturated and remain so throughout time:

$$h_w(x, y, 0) = h(x, y, 0), \quad \frac{\partial h_w}{\partial t}(x, y, t) = \frac{\partial h}{\partial t}(x, y, t)$$

Combining (1.1) and (1.2) then yields a nonlinear elliptic PDE for the potential

$$\nabla \cdot \mathbf{q} + v_o(h) - v_c(h, N) = m \tag{1.4}$$

which is subject to pressure (Dirichlet) boundary conditions on part of the boundary $\partial\Omega_D$ and flux (Neumann) boundary conditions on the remainder of the boundary $\partial\Omega_N$. Neumann boundary conditions take the form

$$\mathbf{q} \cdot \mathbf{n} = q_N$$

where $\mathbf{n}$ is the outward normal vector to the boundary and q_N is some prescribed influx or outflux. Usually, $\phi = \phi_m$ (zero pressure) is prescribed on boundaries where outflow is expected and $\mathbf{q} \cdot \mathbf{n} = 0$ (zero flux) is prescribed elsewhere.

The model is advanced in time by solving the PDE (1.4) with h fixed to obtain ϕ then solving (1.1) with ϕ fixed to advance h in time. On initialization of the model, cavities are assumed to be fully saturated. The PDE ensures that cavities remain saturated by enforcing $\frac{\partial h_w}{\partial t} = \frac{\partial h}{\partial t}$ so that water height and cavity height evolve together. In effect, the hydraulic potential is chosen at each time step to maintain the saturation assumption. It should also be noted that solving for the hydraulic potential is equivalent to solving for the water pressure as water pressure can be easily derived from potential as $p_w = \phi - \phi_m$.

As currently posed, the model is flawed in that the PDE may predict water pressure below zero or well above overburden, which are equivalent to $\phi < \phi_m$ and $\phi > \phi_0$ respectively. Underpressure, or water pressure below zero, is most prevalent on realistic ice sheet geometries near the margin or other regions with thin ice [*Schoof et al.*, 2012]. Underpressure occurs because the model is not properly equipped to deal with partially filled cavities. In a situation where cavities would realistically lose saturation, partially filling with air, the PDE maintains saturation by predicting negative water pressure. Overpressure, or water pressure above overburden, usually occurs in areas with high melt input. Although water pressure above overburden is physically plausible, the model does not include specialized physics for ice uplift that would alleviate extreme overpressure possible in the model. The opening of an ice-water gap is modeled in *Tsai and Rice* [2010] but has yet to be integrated into a more general model.

To remedy these problems, *Schoof et al.* [2012] propose an alternative method for determining hydraulic potential when overpressure or underpressure are present. In such instances, ϕ is determined by minimizing the functional

$$J(\phi) = \int_\Omega \left[\frac{1}{\beta} k h^\alpha |\nabla \phi|^\beta + \frac{1}{4} A h N^4 - (m - v_o(h))\phi \right] d\Omega - \int_{\partial\Omega_N} q_N \phi d\Gamma \qquad (1.5)$$

subject to the constraints $\phi_m \leq \phi \leq \phi_0$ (or equivalently $0 \leq p_w \leq p_i$) and any applied Dirichlet boundary conditions. Minimizing (1.5) subject to constraints always yields a solution for water pressure in a physically plausible range. If no constraints are imposed, minimizing (1.5) is equivalent to solving the PDE (1.4).

Where the solution to (1.5) has regions of zero water pressure or overburden pressure, the rates of change of h_w and h are different and the two variables should technically be solved for separately using the ODE (1.1) and conservation equation (1.2) respectively. However, this requires complicated procedures for dynamically tracking these regions and solving for the two unknowns separately. Since regions of underpressure or overpressure are generally small, we continue to treat cavities as

saturated in these areas and advance both h and h_w using the typical ODE (1.1). Our approach compares to *Bueler and van Pelt* [2014] who also implement a method to prevent underpressure and overpressure but forgo the complexities of solving for h and h_w separately.

1.2.1 Numerical Solution

We have implemented the model posed by *Schoof et al.* [2012] in FEniCS, a finite element package emphasising variational forms, callable form Python or C++ [*Alnæs et al.*, 2015]. All spatially varying fields are discretized using linear Lagrange finite elements. The model must be initialized with an initial cavity height h_0. The standard time stepping procedure involves solving the PDE (1.4) with h fixed, then advancing the ODE (1.1) for h by a given time step with ϕ fixed. The PDE (1.4) is nonlinear and is solved in FEniCS using Netwon's method [*Nocedal and Wright*, 2006]. The ODE (1.1) is solved using a parallel implementation of an implicit Adams method [*Brown et al.*, 1989]. If at any point the solution to the PDE contains under or overpressure regions, ϕ is instead determined by minimizing the functional (1.5) subject $\phi_m \leq \phi \leq \phi_0$ and any Dirichlet boundary conditions using the L-BFGS-B algorithm for solving constrained optimization problems [*Byrd et al.*, 1995]. Since solving the PDE is much less costly than solving the constrained optimization problem, we always solve the PDE first to obtain an initial guess for the optimization algorithm.

1.2.2 Model Limitations

As a reference, we compare modeled pressures to borehole pressure measurements from Isunnguata Sermia [see *Meierbachtol et al.*, 2013, *Wright et al.*, 2016], which typically hover near overburden pressure throughout the winter. It is not clear if the linked cavity model is a good conceptual model of the subglacial drainage system in this region of Greenland or if a multi-element model with channels [e.g. *Werder et al.*, 2013] or till [*Bueler and van Pelt*, 2014] might be more suitable. There is

some evidence to support a distributed modeling approach versus one with explicit channelization. For example, *Meierbachtol et al.* [2013] have argued that the distance channels propagate into the ice sheet interior is limited based on borehole measurements and numerical experiments. Similarly, *Andrews et al.* [2014] noted that few borehole pressure measurements have been obtained for channelized regions of the bed, which they attribute to both the scarcity of borehole measurements as well the limited spatial influence of channels on water pressure.

It is also unclear if the omission of sediment is an important one. Borehole measurements indicate that the drainage system under Isunnguata Sermia is characteristic of a hard bed [*Harper et al.*, 2015]. Further south, *Dow et al.* [2013] have found seismic evidence of sediment underlying Russel glacier. However, the spatial extent and thickness of till is largely unknown. Beyond the omission of some drainage elements there are broader limitations that apply to any model with a linked cavity component. *Hoffman and Price* [2014] provide a thorough discussion of these limitations including uncertainties in the flux relation and rate of creep closure.

1.3 Synthetic Experiments and Results

In the following model experiments on synthetic geometries, we explore the sensitivity of winter water pressure to bed geometry, hydraulic conductivity, and sliding speed. All synthetic experiments are conducted on a 60 x 20 km model domain. Discretized equations are solved on a mesh with triangular elements having circumradii of ∼500 m. A plastic ice-sheet surface profile [*Cuffey and Patterson*, 2010, chap. 8] with a maximum thickness of 1500 meters (≈ 167 kPa yield stress) is used for ice sheet thickness. A zero pressure ($\phi = \rho_w g B$) boundary condition is applied at the terminus ($x = 0$) and zero flux applied at the remaining boundaries. All synthetic model inputs are shown in figure 1.2. In subsequent experiments we record pressure at the three test points indicated in figure 1.2 (a), which are intended to capture the spatial variability in water pressure. In contrast to previous studies such as *Hoffman*

and Price [2014] and *Hewitt.* [2013] that couple basal hydrology models to ice sheet models, we do not model ice sheet dynamics. Basal sliding speed and ice thickness are prescribed.

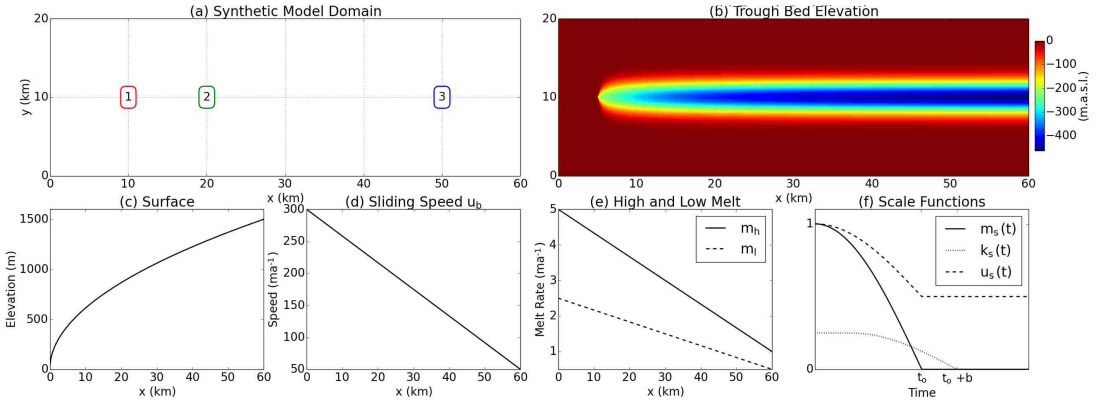

Fig. 1.1.: This figure shows all synthetic model inputs. (a) Synthetic experiments share a 60 x 20 km model domain with 0 pressure applied at the margin ($x = 0$km) and 0 flux applied at all other boundaries. 1, 2, and 3 are points where pressure is recorded for subsequent plots. (e) High melt m_h and low melt m_l variants (f) This panel shows scaling functions used for time variable melt, conductivity, and sliding speed functions. t_0 is the shut off time when melt reaches 0. b is lag time of conductivity behind melt.

1.3.1 Reference Experiment (REF)

In this experiment, we simulate winter water pressure on both a flat bed and trough. We allow both model runs to reach a steady state with persistent melt input m_h. Melt is then reduced during the melt shut off period by multiplying melt rate by a scaling function

$$m_s(t) = \max\left(\cos\left(\frac{\pi t}{2t_o}\right), 0\right) \tag{1.6}$$

with a shut off time parameter t_o that controls when melt ceases. Here, we use a shut off time of one month. Additional model inputs and parameters for the flat bed and trough runs (REF FB and REF T) are listed in table 1.3. Parameter values are based on *Schoof et al.* [2012], *Werder et al.* [2013], and *Hewitt et al.* [2012]. We use default

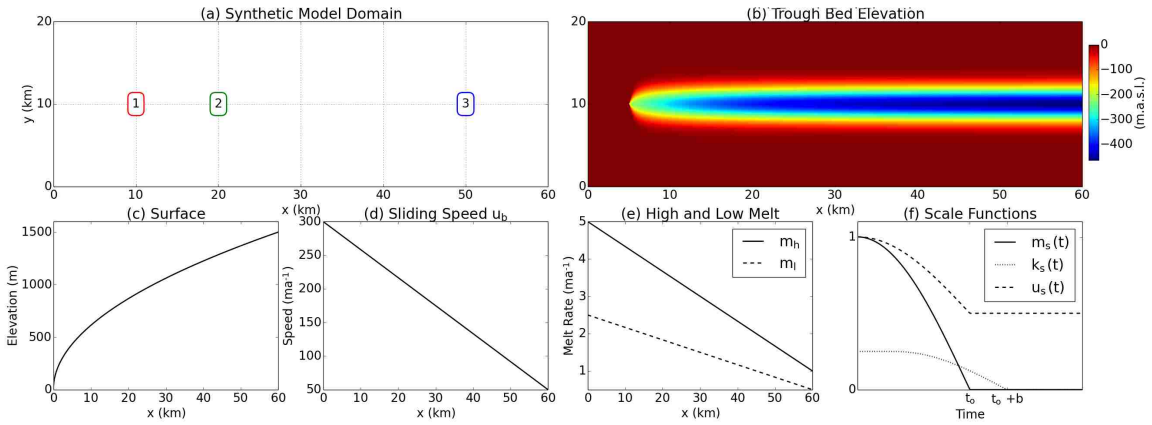

Fig. 1.2.: This figure shows all synthetic model inputs. (a) Synthetic experiments share a 60 x 20 km model domain with 0 pressure applied at the margin ($x = 0$km) and 0 flux applied at all other boundaries. 1, 2, and 3 are points where pressure is recorded for subsequent plots. (e) High melt m_h and low melt m_l variants (f) This panel shows scaling functions used for time variable melt, conductivity, and sliding speed functions. t_0 is the shut off time when melt reaches 0. b is lag time of conductivity behind melt.

values of 0.1m for h_r and 2m for l_r. k is selected to produce sensible summer steady state water pressures around overburden pressure. In our reference runs, sliding speed is time invariant. Winter water pressures at the three test points are plotted in figure 1.3.

The reference experiment highlights a significant disparity between modeled and observed water pressures. Whereas borehole observations hover around overburden pressure through the winter, modeled pressures plummet. In the flat bed run, pressures at the three test points approach zero by the end of winter. Pressures remain higher in in the trough run – between 26-40% of overburden pressure – due to melt water retention in the trough. Even so, spatially averaged pressure decreases by almost 85% from the summer steady state to the end of winter.

Certainly, we should not expect the model to closely agree with observations in this highly simplified scenario. However, we do not see even broad agreement. In the following experiments, we test a number of factors that might contribute to this

problem including unrealistic model inputs in the form of sliding speed and ice sheet geometry as well as poorly constrained parameters.

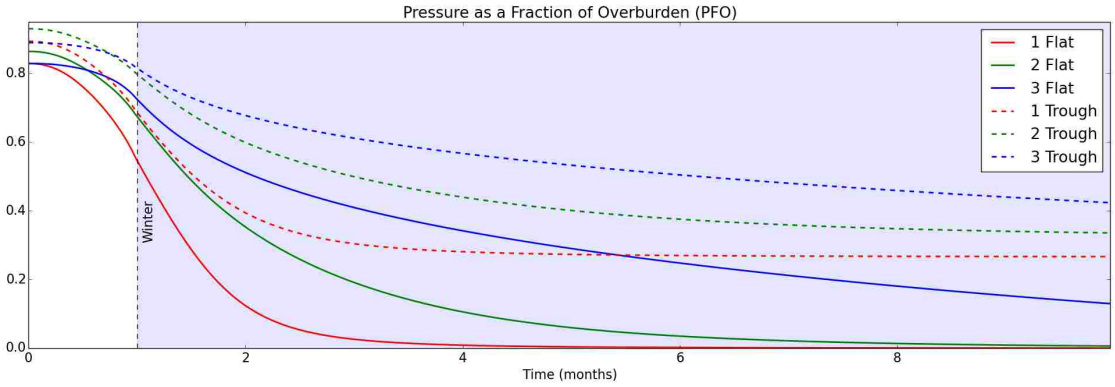

Fig. 1.3.: This figure shows the rapid fall of winter water pressures with standard model parameters. Solid lines indicates pressures for the flat bed run (REF FB) while dashed lines are for the trough run (REF T). Colors correspond to the three test points shown in figure 1.2 (a)

.

1.3.2 Sliding and Bump Parameter Experiment (SBP)

The sliding speed used in the reference experiment is appropriate for summer but too high for winter in Isunnguata Sermia [*Bartholomew et al.*, 2010]. Large values of u_b correspond to a large cavity opening rate which in turn reduces water pressure. The cavity opening rate also depends on uncertain values of the bedrock bump parameters h_r and l_r. Hence, it might be that low winter pressure is caused by a combination of unrealistic bump parameters and sliding speed.

In the following experiment, we test this idea by simulating winter pressure on a trough with sliding speed decreasing as a function of time and a range of bedrock bump parameters. We perform nine total runs with bump heights of 0.05, 0.1, and 0.5m in combination with bump lengths of 1, 2, and 5m. These values span the range of bedrock bump parameters used in publications including *Schoof et al.* [2012], *Werder et al.* [2013], *Hoffman and Price* [2014], *Hewitt.* [2013], and *Bueler and van*

Pelt [2014]. To compensate for changes in bump height or spacing, the conductivity is altered to assure that the modeled summer pressures are comparable to borhole observations. In each run, spatially averaged summer steady state pressure is around 80% of overburden pressure. Conductivity values used in each run are shown in table 1.2.

All runs use the same time variable sliding speed u_b^* given by

$$u_b^*(t) = u_s(t)u_b(x, y) \tag{1.7}$$

where $u_s(t)$ is a scaling function defined by

$$u_s(t) = m_s(t)\left(1 - \frac{u_{max}}{\max(u_b)}\right) + \frac{u_{max}}{\max(u_b)}.$$

Here u_{max} is the maximum desired winter sliding speed. When the melt scaling function $m_s(t)$ is 1, $u_b^* = u_b$ and when $m_s(t) = 0$, the maximum value of u_b^* at any point is u_{max}. We impose a realistic u_{max} for Isunnguata Sermia of 100 ma^{-1}.

Table 1.2: Constant k values (units m$^{7/4}$kg$^{-1/2}$) for each run in the SBP experiment with a different combination of the bump height parameters. Conductivity values are adjusted so that spatially averaged summer steady state pressure in each run is near 80% of overburden pressure.

		$\mathbf{l_r}$		
		1m	2m	5m
$\mathbf{h_r}$	0.05m	1.1×10^{-2}	1.33×10^{-2}	2.1×10^{-2}
	0.1m	4.65×10^{-3}	5.2×10^{-3}	8.5×10^{-3}
	0.5m	6.2×10^{-4}	7.3×10^{-4}	1.16×10^{-4}
	1m	2.55×10^{-4}	3.05×10^{-4}	4.75×10^{-4}
	2m	-	-	2×10^{-4}

Figure 1.4 shows that reducing sliding speed is not sufficient to maintain high winter pressure regardless of the values of the bedrock bump parameters. Different

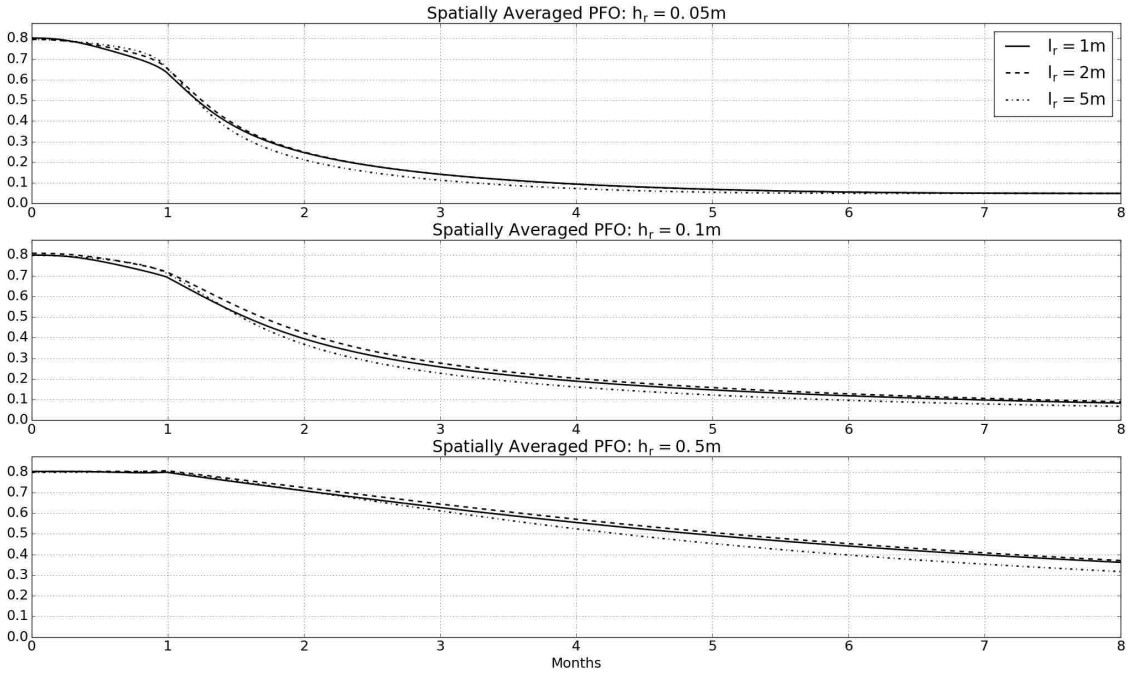

Fig. 1.4.: Each panel shows spatially averaged pressures for a specific bump height h_r and various bump lengths l_r. In each model run, sliding speed is time variable.

.

bump lengths cause only miniscule changes in spatially averaged winter pressure. In contrast, there is a clear trend between larger bump heights and higher winter pressure. Spatially averaged pressures fall to around 10% of overburden pressure in each of the 0.05 and 0.1m runs, though the decline in pressures in early winter is more gradual in the 0.1 meter runs. For a bump height of 0.5m, spatially averaged pressures drop to 30-40% of overburden pressure by the end of winter. While these pressures are still well below borehole observations, it is worth asking why they are higher when compared to runs with lower bump heights.

The relationship between bump height and winter pressure seems counterintuitive. Taller bedrock bumps increase the cavity opening rate which should reduce water pressure. Indeed, increasing h_r reduces pressure if hydraulic conductivity is fixed. Therefore, runs with larger bump heights have unrealistically low summer steady state water pressures unless unless k is decreased to compensate. It is not large

values of h_r but low values of k contributing to higher pressures in the 0.1 and 0.5m bump height runs.

These results suggest that one approach to remedying low winter pressure might be to further increase h_r and impose a smaller constant value of k. Along these lines, we performed four additional runs with large bump heights. The first three runs used an h_r of 1m combined with l_r values of 1, 2, and 5m. Conductivities for these runs are also shown in table 1.2. Spatially averaged pressures fell by nearly 30% by the end of winter in each run. We then performed a run with an h_r of 2m (well beyond what has been used in other publications) and l_r of 5m. Spatially averaged pressure remained closer to observations, dropping only around 17% by the end of winter. Nonetheless, this run tests the limits of what is physically plausible in other respects. Due to low conductivity, summer steady state sheet height h exceeded 1m over roughly a third of the spatial domain. Since h is a spatial average and water is not distributed uniformly at the bed, this would require large, potentially multi-meter tall cavities in these areas. Much of the annual melt input is stored in the sheet.

1.3.3 Time Varying Conductivity and Sliding

Perhaps a more physically plausible solution to low winter pressure not contingent on imposing a large bump height would be to allow conductivity to decrease over time. In the following two experiments, conductivity mimics melt input both spatially and temporally. In particular k is now a a function of the form

$$k = k_s(t)m(x, y) + k_{min} \tag{1.8}$$

where k_{min} is some prescribed minimum conductivity and $k_s(t)$ is a conductivity scale function that mimics the melt scale function $m_s(t)$. The conductivity scale function has the form

$$k_s(t) = \left(\frac{k_{max} - k_{min}}{\max(m)}\right) m_s(t - b) \tag{1.9}$$

where k_{max} is highest attainable conductivity, and b is the lag of conductivity behind melt. The highest possible conductivity is achieved when and where melt is at its highest. When melt ceases, conductivity simply becomes a constant k_{min}. The idea is that decreasing melt leads to reduced conductivity. We interpret this change in conductivity as reflecting subgrid scale changes in drainage system geometry. These small-scale geometric changes reduce the connectivity of the linked cavity system and therefore discharge. In effect, we adopt conductivity as a proxy for drainage system connectivity.

Shut Off Time Experiment (ST)

We now simulate winter water pressure on a flat bed with sliding speed and conductivity related to melt input via equations (1.7) and (1.8) respectively. We perform six model runs – three runs with high melt input m_h (ST HM) and varying shut off times t_o of a day, week, and month. We then perform three similar runs (ST LM) with low melt input m_l (see table 1.3). Figure 1.5 shows that reducing conductivity in concert with melt produces high winter water pressures broadly consistent with observations. For all three shut off times tested, pressures exhibit a similar pattern characterized by a small spike during the melt shut off period followed by a gradual decline over the winter. One consequence of linking conductivity to melt spatially as in equation (1.8) is that there is little difference between pressures in the high and low melt runs. Any pressure increase that might result from additional melt input is offset by higher conductivity.

The shut off time experiment verifies that changing conductivity is an effective way to prevent low winter pressure. It also serves as a first attempt at finding bounds on k by comparing the model with borehole observations. Both the summer upper bound k_{max} and the winter lower bound k_{min} on conductivity are chosen to yield sensible pressures. If k is too high at any point in time, pressures drop unrealistically low. On the other hand, there is perhaps no identifiable minimum value for k since if

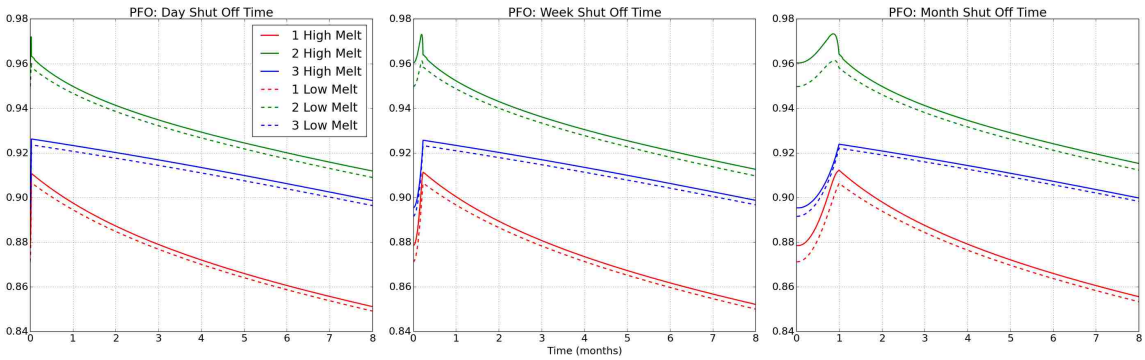

Fig. 1.5.: Each panel shows the results of a high melt and low melt model run in the ST experiment with a with a particular shut off time. Solid lines indicate pressures for the high melt experiments and dashed lines for the low melt experiments. Colors correspond to the three standard test points.

k_{min} is too low, pressure rises to overburden over most of the domain in which case the pressure constraints in the model apply.

Lag Time Experiment (LT)

Changes in melt input may not immediately impact the connectivity of the linked cavity system. Therefore, it may be sensible to delay the response of conductivity to melt by imposing a nonzero lag time b in the conductivity scale function (1.9). This experiment tests the impact of lag time on winter water pressure and storage. The setup is essentially the same as the shut off time experiment ST except that we now test three lag times b of a day, week, and month with a fixed shut off time t_o of one month for both high (LT LM) and low melt input (LT HM). Figures 1.6 and 1.7 display winter pressures and water storage respectively for different lag times.

Figure 1.6 shows that long lag times of multiple weeks to a month are improbable. A lag time of one day yields consistently high pressures resembling those in the shut off time experiment ST. As lag time is extended, pressures drop during the period of high conductivity but decreasing melt input. This effect is small in the week lag test where pressures drop by only around 2-12% but more pronounced in the month lag

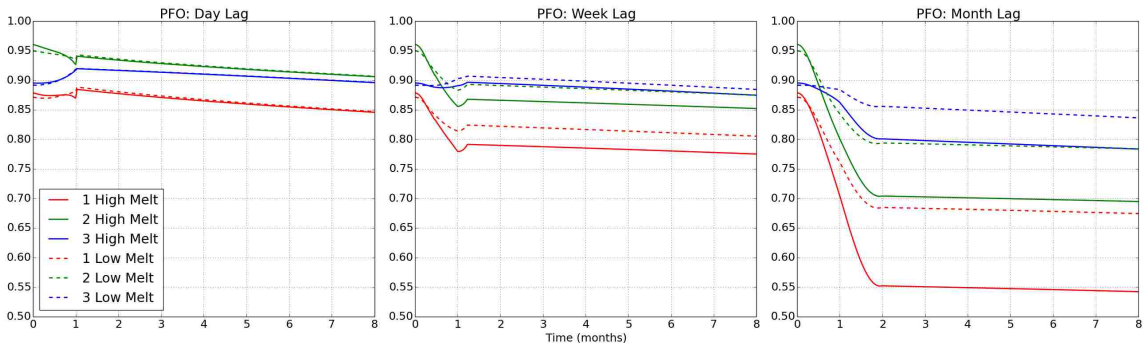

Fig. 1.6.: Each panel shows the results of a high melt and low melt model run in the LT experiment with a with a particular lag time b. Solid lines indicate pressures for the high melt runs and dashed lines for the low melt runs. Colors correspond to the three standard test points.

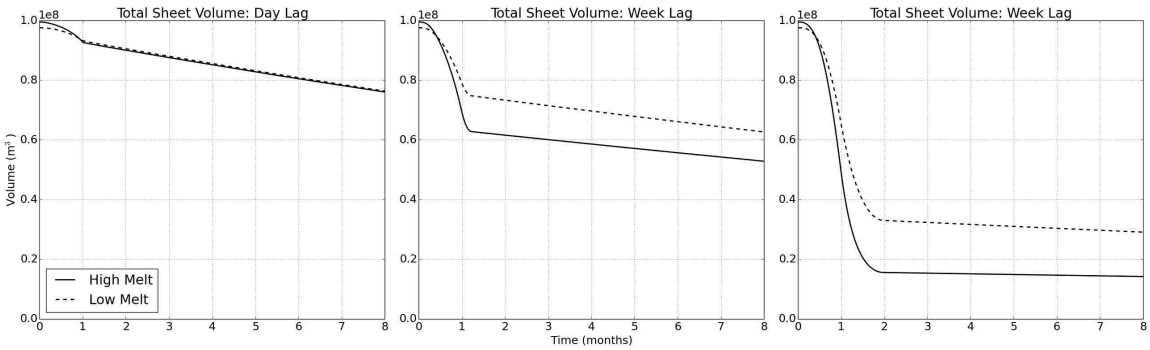

Fig. 1.7.: Each panel shows the total sheet volume for the high and low melt runs in the LT experiment with a particular lag time. High melt sheet volume is indicated with a solid line and low melt volume with a dashed line.

test where pressures drop by up to 23% in the low melt run and up to 38% in the high melt run.

Unlike the shut off time experiment where the quantity of summer melt input was essentially irrelevant, there is a notable difference in pressures between the high and low melt variants of the week and month lag tests. This difference can be attributed to the spatial dependence of conductivity on melt. Initial summer conductivity is higher in the high melt scenario. Consequently, during the melt shut off period, stored water in the sheet drains rapidly and pressure drops substantially as shown in figuire 1.7.

In contrast, sheet drainage is less rapid and the associated pressure drop less severe for the low melt scenario since the initial summer conductivity is lower.

1.4 Realistic Experiments and Results

In the preceding synthetic experiments, we showed that reducing hydraulic conductivity can reproduce observed high winter water pressures on synthetic geometries. In the final three experiments, we test if this result is robust for a more complicated ice sheet geometry by applying the model to Isunnguata Sermia in Western Central Greenland. For model inputs, we use measurements of bed elevation and ice thickness from *Bamber et al.* [2013], accumulation from *SeaRISE* [2012], and surface velocity from *Rignot and Kanagaratnam* [2006]. All model inputs are plotted in figure 1.8. We again use a numerical mesh with a spatial resolution of ∼500 m. In place of the true margin we define the left edge of the domain to be the 50m ice thickness contour line (indicated by the dashed line in figure 1.8(c)). Imposing a minimum ice thickness of 50m helps prevent excessively large cavity opening rates in the ODE (1.1) due to high sliding speeds and low creep closure rates near the margin.

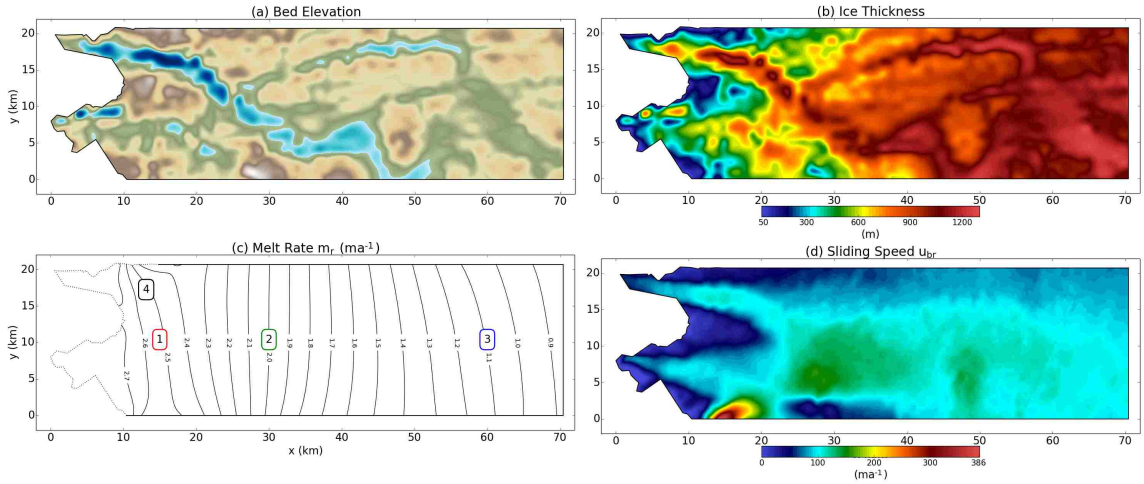

Fig. 1.8.: This figure shows inputs for realistic model runs on Isunnguata Sermia. (c) The dashed line indicates the 50 meter ice thickness contour where a zero pressure Dirichlet boundary condition is applied. Zero flux is applied on all other boundaries. 1, 2, 3, and 4 are points where pressure will be recorded for experiments on realistic geometry. (d) Sliding speed is taken to be the observed surface velocity.

Summer surface velocities exceed 100 ma^{-1} throughout much of the domain. Hence, we assume that most ice motion can be attributed to basal sliding and use surface velocity for the summer sliding speed. For simplicity, we also assume that all surface melt is routed directly to the underlying bed. Modeled water pressures on a realistic bed tend to be spatially heterogeneous. Therefore we supplement water pressure time series recorded at the four test points shown in figure 1.8(c) with a number of 2D plots.

1.4.1 Reference Experiment on Realistic Geometry (REFR)

We now replicate the reference experiment (REF) on a realistic ice sheet geometry, simulating winter pressures with time invariant sliding speed and constant k. Water pressures at the four test points are shown in figure 1.9. Summer steady state and end of winter water pressure fields are plotted in figure 1.10.

Realistic ice sheet geometry creates complex temporal and spatial patterns in water pressure. Pressures at the first three test points resemble earlier runs on a

synthetic bedrock trough, dropping by around 40 - 50% before leveling out in late winter. Curiously, water pressure at the fourth test point drops by only around 5%. Examining figure 1.10 shows that this test point is situated in one of two perennially pressurized bedrock troughs. Steep bed gradients route water into troughs while the reverse bed slope near the margin limits outflow. In spite of these high pressure features, the spatially averaged water pressure falls by almost 50% over the 7 months simulated. Although bedrock geometry creates high pressure regions, it is clear that changing conductivity and sliding speed is necessary to produce high water pressure over a most of the domain.

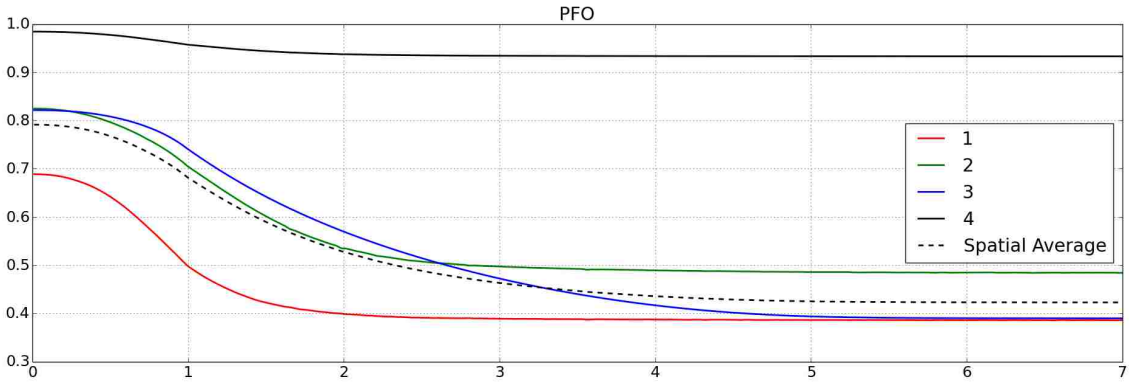

Fig. 1.9.: This figure shows winter water pressures for the REFR experiment on a realistic geometry with constant conductivity and time invariant sliding speed. Colors correspond to the four test points shown in 1.8 (c).

1.4.2 Time Variable Sliding on Realistic Geometry (TVSR)

As in earlier synthetic runs, we found that reducing sliding speed without also reducing conductivity is not sufficient to maintain high winter pressure on a realistic geometry. To test this we simulated winter pressure on a realistic geometry with time variable sliding and fixed k. Results are not plotted since they mimic results from previous experiments. Pressures at points 2, 3, and 4 remained relatively steady during the melt shut off period while pressure at the first test point dropped by around

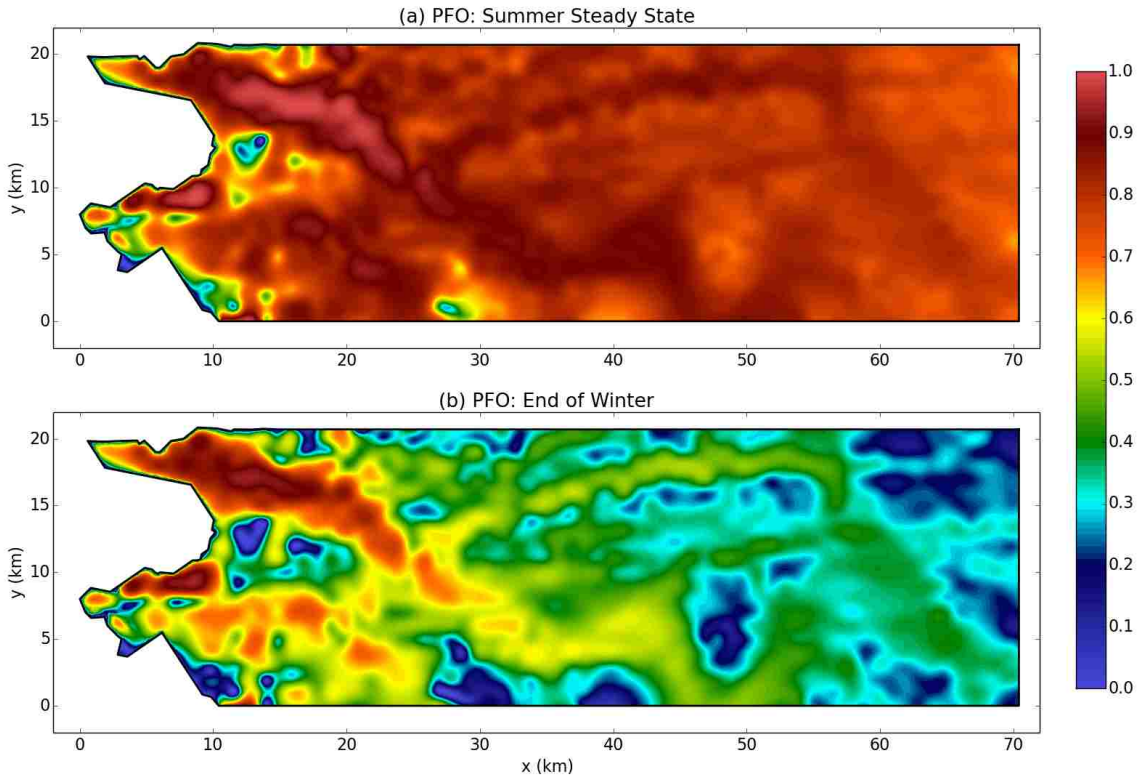

Fig. 1.10.: This figure shows summer and winter pressures on a realistic ice sheet geometry for the REFR experiment with constant conductivity and time invariant sliding speed. (a) shows the end of summer steady state pressure and (b) shows the end of winter pressure.

45 %. After melt ceased, pressures plummeted at test points 1, 2, and 3. Comparable to REFR, spatially averaged pressure dropped by nearly 50% after 7 months.

1.4.3 Time Dependent Sliding and Conductivity on Realistic Geometry (TDSCR)

Finally, we simulate winter water pressure on a realistic ice sheet geometry with time dependent conductivity and sliding speed. Figures 1.11 and 1.12 confirm that, as in earlier synthetic test cases, reducing conductivity and sliding speed with melt input yields high winter pressure across most of the spatial domain. Spatially averaged water pressure remains between 80-90% of overburden pressure throughout the winter.

Table 1.3: This table shows important model inputs and parameters for each model experiment. Some experiments involve multiple model runs with different inputs indicated by a suffix after the experiment abbreviation. Some experiments also involve multiple runs using the same model inputs but different parameters. Where applicable, the number of runs and any varied parameters are indicated. All runs start from a summer steady state. Unless otherwise stated, runs use default values of 10cm for h_r and 2m for l_r.

Name	**B** (m)	$\mathbf{m(x,y)}$	$\mathbf{t_o}$	$\mathbf{u_b(x,y)}$	**k**	**Figs.**
REF FB	flat	m_h - Fig. 1.2 (e)	month	u_b - Fig. 1.2 (d)	5×10^{-3}	1.3
Simulates winter pressure on a flat bed with time invariant sliding speed and constant k.						
REF T	trough - Fig. 1.2 (b)	m_h - Fig. 1.2 (e)	month	u_b - Fig. 1.2 (d)	5×10^{-3}	1.3
Similar to REF FB except on a trough bed geometry.						
SBP (×9)	trough - Fig. 1.2 (b)	m_h - Fig. 1.2 (e)	month	u_b - Fig. 1.2 (d)	constant, varies	1.4
9 runs with h_r values of 0.05, 0.1, and 0.5m in combination with l_r values of 1, 2, and 5m. Sliding speed is time variable following eq. (1.7) with $u_{max} = 100$ ma^{-1}. Conductivity is adjusted in each run to attain an average summer steady state pressure of 80% of overburden pressure. Conductivity values for each run are shown in table 1.2.						
ST LM (×3)	flat	m_l - Fig. 1.2 (e)	varies	u_b - Fig. 1.2 (d)	time/spatially variable	1.5
3 runs with melt shut off times t_0 of a day, week, and month. Sliding speed follows eq. (1.7) with $u_{max} = 100$ma^{-1}, and conductivity follows eq. (1.8) with $k_{min} = 5 \times 10^{-5}$ and $k_{max} = 5 \times 10^{-3}$.						
ST HM (×3)	flat	m_h - Fig. 1.2 (e)	varies	u_b - Fig. 1.2 (d)	time/spatially variable	1.5
3 similar runs to ST LM except with higher melt input.						
LT LM (×3)	flat	m_l - Fig. 1.2 (e)	month	u_b - Fig. 1.2 (d)	time/spatially variable	1.6, 1.7
3 runs with conductivity lag times b of a day, week, and month. Sliding speed follows eq. (1.7) with $u_{max} = 100$ma^{-1}, and conductivity follows eq. (1.8) with $k_{min} = 5 \times 10^{-5}$ and $k_{max} = 5 \times 10^{-3}$.						
LT HM (×3)	flat	m_h - Fig. 1.2 (e)	month	u_b - Fig. 1.2 (d)	time/spatially variable	1.6, 1.7
3 similar runs to LT LM except with higher melt input.						
REFR	real - Fig. 1.8 (a)	m_r - Fig. 1.8 (c)	month	u_{br} - Fig. 1.8 (d)	5×10^{-3}	1.9, 1.10
Repeat of REF experiment with constant k and time invariant sliding on realistic geometry.						
TVSR	real - Fig. 1.8 (a)	m_r - Fig. 1.8 (c)	month	u_{br} - Fig. 1.8 (d)	5×10^{-3}	-
Simulates winter pressure on realistic geometry with time variable sliding but constant k. Sliding speed follows eq. (1.7) with $u_{max} = 100$ma^{-1}.						
TVCSR	real - Fig. 1.8 (a)	m_r - Fig. 1.8 (c)	month	u_{br} - Fig. 1.8 (d)	time/spatially variable	1.11, 1.12
Simulates winter pressure on realistic geometry with time variable sliding and conductivity. Sliding speed follows eq. (1.7) with $u_{max} = 100$ma^{-1}, and conductivity follows eq. (1.8) with $k_{min} = 7 \times 10^{-5}$ and $k_{max} = 7 \times 10^{-3}$.						

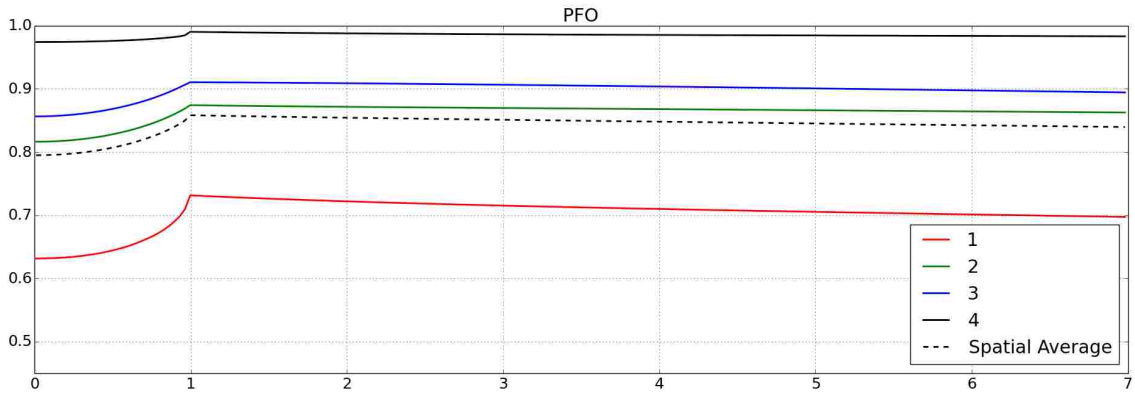

Fig. 1.11.: This figure shows winter pressures for the TVCSR experiment on a realistic ice sheet geometry where conductivity and sliding speed vary over time. Colors correspond to the four test points shown in 1.8 (c).

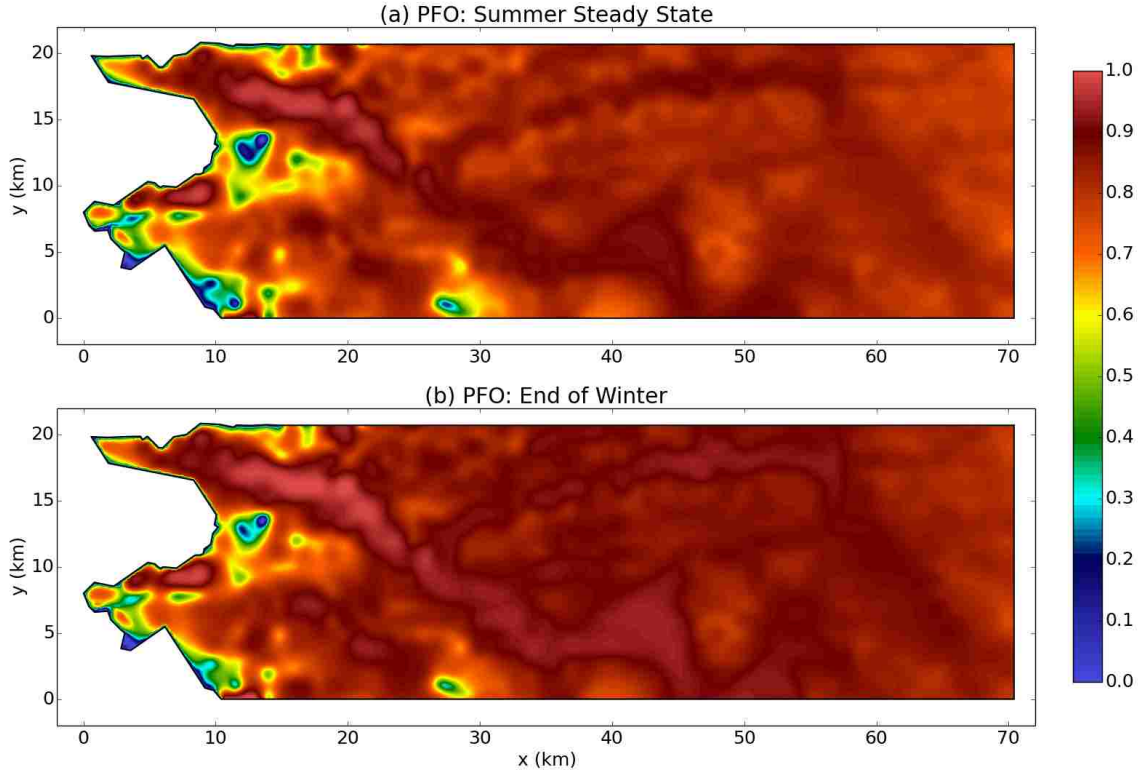

Fig. 1.12.: This figure shows summer and winter pressure for the TVCSR experiment on a realistic ice sheet geometry where conductivity and sliding speed vary over time. (a) shows the end of summer steady state pressure and (b) shows the end of winter pressure.

1.5 Discussion

1.5.1 Physical Motivation for Changing Conductivity

In our reference experiment, we presented two simple synthetic simulations in which the model severely underpredicts winter water pressure when compared to borehole observations. While these synthetic runs are not intended to be physically realistic, they demonstrate that high winter water pressure is not a natural byproduct of the model physics. That is, the model does not automatically predict high winter pressure given standard model parameters and a time invariant sliding speed. This is not necessarily an intuitive result. It would seem feasible that creep closure might balance with reduced melt input to prevent any substantial drop in modeled water pressure. However, this is clearly not the case.

We identified a number of possible causes of low winter pressure from unrealistic model inputs in the form of sliding speed and ice sheet geometry to poorly constrained parameters including bedrock parameters and hydraulic conductivity. Numerical experiments demonstrated that the model is not sensitive enough to most of these inputs and parameters to explain high winter pressure with the exception of hydraulic conductivity. High winter pressure can be attained by imposing a large bump height in conjunction with a low constant conductivity. This approach requires a bump height value well above what has been used in other publications and results in an implausible sheet thickness. Alternatively, high winter can be attained by decreasing conductivity over time. There is ample numerical evidence to show that varying k in space and time raises winter pressure, but there is clear physical justification as well.

To motivate why the model underpredicts pressure and why changing conductivity is a reasonable solution, consider that a tacit assumption in *Schoof et al.* [2012] is that the dynamics of the linked cavity system are in some sense simpler on large spatial scales than small ones. The idea is that fields such as spatially averaged water pressure and sheet height can be accurately predicted without simulating fine scale features of the bedrock or linked cavity system. For example, the flux relation (1.3)

describes aggregate flow through a patch of the bed a fraction of a square kilometer containing many invididual links and cavities overlying bumpy bedrock. Yet, it has only an implicit dependence on the complex, subgrid-scale geometry of the ice and bedrock via the geometric factor $kh^{\alpha-1}$, where k usually taken to be constant. This geometric factor is perhaps flawed in that it fails to capture small scale changes in the shape and interconnectivity of cavities that affect discharge and pressure.

Observed borehole pressures likely remain high due to reduced connectivity of the drainage system over the winter. Drainage system connectivity depends on small scale features of the ice and bedrock geometry that cannot be explicitly accounted for in the model. To circumvent this issue, hydraulic conductivity k can be used as a proxy for connectivity. Given that small scale bedrock features parameterized through h_r and l_r are included in the creep closure term in equation (1.1), it is also sensible to parameterize the effect of small scale drainage system geometry on discharge. Physically, changes in conductivity reflect changes in the local drainage system geometry due to the opening and closing of links or alterations to the shape of cavities. These geometric changes affect aggregate flux through a patch of the linked cavity system. High values of k represent a well connected section of the linked cavity system with high discharge while low values represent a more isolated section with low discharge.

1.5.2 Constraining Conductivity

Ideally, we might account for changes in connectivity in an elegant way by revising the geometric factor $kh^{\alpha-1}$ in the flux relation – perhaps by expressing k in terms of the other model unknowns such as h. One precedent is provided by *Flowers and Clarke* [2002] who employ a sheet height dependent conductivity for a porous sediment layer. Another possibility might be to increase the exponent α to reduce discharge when sheet height is low. However, it is not clear what functional form the geometric factor should take. Tying conductivity to melt as in equation (1.8) is, though not

an ideal solution, a practical alternative to modeling the complex physics controlling conductivity. It qualitatively captures the idea that reduced melt input corresponds to a low discharge, disconnected drainage system caused by the closure of links or changes to the shape of cavities.

Experiments involving temporally and spatially variable conductivity show that equation (1.8) works well in practice at keeping water pressure broadly in line with observations given a suitable summer upper bound k_{max} and and winter lower bound k_{min} on conductivity. Approximate upper and lower bounds can be obtained by comparing the model to observations. One such approach is outlined by *de Fleurian et al.* [2014] who use observations of a Swiss glacier to tune hydraulic transmissivity, a field closely related to conductivity. Along similar lines, we compare modeled pressures to borehole measurements in *Wright et al.* [2016] and *Meierbachtol et al.* [2013] to obtain rough estimates for summer and winter conductivity. Variations between models mean that a suitable conductivity range in one model is not necessarily applicable to another model. For example, *de Fleurian et al.* [2014] use a linear flux relation versus the nonlinear turbulent flux relation of *Schoof et al.* [2012]. The units and physical meaning of conductivity are tied to the specific model conceptualization.

Schoof et al. [2012] and related models such as *Werder et al.* [2013] and *Bueler and van Pelt* [2014] have used constant conductivity values on the order of 10^{-2} to 10^{-4} $\mathrm{m}^{7/4}\mathrm{kg}^{-1/2}$ depending on the simulation. We found that a value in the middle of this range, 5×10^{-3} $\mathrm{m}^{7/4}\mathrm{kg}^{-1/2}$, is a good baseline for summer conductivity for both synthetic and realistic runs that use a default bump height of 0.1m. Table 1.2 provides a starting point for obtaining reasonable k_{max} values for alternative bump height values. Most previous work has focussed on modeling the melt season rather than the winter phase of the drainage system. For this reason, we are left to guess a suitable minimum value k_{min}. We chose a minimum value of 10^{-5} $\mathrm{m}^{7/4}\mathrm{kg}^{-1/2}$ – two orders of magnitude lower than the summer high conductivity. Low winter conductivity values in this range could probably be achieved in a poorly connected linked cavity system.

1.5.3 Implications for Sliding

Sole et al. [2013] have shown that fast ice flow in high melt summers is offset by slower flow in subsequent winters. They hypothesize that a well developed channel system after high melt summers remains partially open during the winter, lowering net water pressure and decreasing sliding speed. In contrast, a less developed drainage system after a low melt summer is associated with higher net winter pressure and faster sliding. However, borehole pressure measurements generally remain high throughout the fall and winter, indicating that sliding speed depends on the quantity and distribution of water in the drainage system as well as pressure.

The lag time experiment suggests that this phenomenon could alternatively be explained by differences in winter water storage caused by a slight lag in conductivity behind melt. Although long lag times of multiple weeks to a month are implausible because they cause an unrealistic drop in water pressure, shorter lag times around a week are feasible. The drainage system must respond relatively quickly to reduced melt input or we would likely see a similar drop in borehole pressures. Figure 1.6 shows that a week lag time causes a noticeable ($\approx 16\%$) difference in winter water storage after high and low melt summers. In particular, the low melt summer is followed by a high storage winter and vice versa.

High melt summers result in a well connected and efficient linked cavity system. Stored water in the sheet drains quickly before the linked cavity system becomes largely disconnected in the winter. After low melt summers, the linked cavity system is not as well connected. Less stored water drains during the melt shut off period before the linked cavity system transitions to a mostly isolated system. Thus, slow ice flow after a high melt summers could be caused predominantly by low winter water storage rather than low pressure.

1.5.4 Conclusions and Future Work

We have shown that a common model of subglacial drainage through linked cavities underpredicts winter pressure when compared to borehole observations. Through a series of model experiments, we determined that the most feasible solution to this problem is to allow hydraulic conductivity to vary both spatially and temporally. Variations in melt input result in changes to the connectivity and efficiency of the linked cavity system that are not captured in the model if conductivity is constant.

Our results support the idea that differences in sliding speed following high or low melt summers are driven primarily by differences in winter water storage rather than pressure. High melt summers lead to a well connected cavity system that drains quickly as melt input decreases provided there is a slight (approximately 1 week) delay between reduced melt input and reduced conductivity. Low melt summers lead to a less efficient cavity system that drains more slowly. Consequently, there is less winter storage after a high melt summers than low melt summers. These differences in storage are possible without significant differences in winter pressure.

Additional work may be needed to assess the impact of channels on winter pressure and water storage. We expect that our primary conclusion – that reducing hydraulic conductivity is the most feasible way of preventing low winter pressure – will apply directly to channel models. How channels might impact winter water storage after high and low melt summers is difficult to predict. Further work is also needed to refine the geometric factor $kh^{\alpha-1}$ in the flux relation. Small scale models that simulate individual links and cavities could be used to devise an improved aggregate flux relation that accounts for changing drainage system connectivity. Physical processes often neglected in large scale models such as dissipative opening and refreezing of links or ice uplift could be important. Until the physical processes controlling conductivity are better understood, tuning models to match observations such as we have done here done here, or inverse methods may be used to constrain the conductivity.

1.6 Code Repository

The sheet model implementation used in this paper is available at `https://github.com/JacobDowns/SheetModel`. A collection of model experiments found in this paper is also available at `https://github.com/JacobDowns/SheetExperiments`.

Bibliography

Alnæs, M. S., J. Blechta, J. Hake, A. Johansson, B. Kehlet, A. Logg, C. Richardson, J. Ring, M. E. Rognes, and G. N. Wells (2015), The FEniCS Project Version 1.5, 3(100), doi:10.11588/ans.2015.100.20553.

Andrews, L., G. Catania, M. Hoffman, J. Gulley, M. Lüthi, C. Ryser, R. Hawley, T. Neumann (2014), Direct observations of evolving subglacial drainage system beneath the Greenland Ice Sheet *Nature*, 514, 80-83, doi:10.1038/nature13796.

Bamber, J., J. Griggs, R. Hurkmans, J. Dowdeswell, S. Gogineni, I. Howat, J. Mouginot, J. Paden, S. Palmer, E. Rignot, D. Steinhage (2013), A new bed elevation dataset for Greenland *Cryosphere*, 7, 499-510, doi:10.5194/tc-7-499-2013.

Bartholomew, I., P. Nienow, D. Mair, A. Hubbard, M. King, A. Sole (2010), Seasonal evolution of subglacial drainage and acceleration in a Greenland outlet glacier *Nature Geosci. Let.*, 3, 408-411, doi:10.1038/ngeo863.

Bindschadler, R. (1983), The importance of pressurized subglacial water in separation and sliding at the glacier bed *J. Glac.*, 29, 3-19, doi:10.3198/10.3198/1983JoG29-101-3-19.

Brown, P. N., G. Byrne, A. Hindmarsh (1989), VODE: A variable-coefficient ODE solver *SIAM J. Sci. Stat. Comput.*, 10, 1038-1051

Budd, W. F., P. Keage, N. Blundy (1979), Empirical studies of ice sliding *J. Glac.*, 23, 157-170, doi:10.3198/1979JoG23-89-157-170.

Bueler, E., W. van Pelt (2014), Mass-conserving subglacial hydrology in the Parallel Ice Sheet Model version 0.6 *Geosci. Mod. Dev.*, 7, 4705-4775, doi:10.5194/gmdd-7-4705-2014.

Byrd, R., P. Lu, J. Nocedal (1995), A limited memory algorithm for bound constrained optimization *SIAM J. Sci. and Stat. Comp,*, 16, 1190-1208, doi:10.1137/0916069.

Clarke, G. (1996), Lumped-element analysis of subglacial hydraulic circuits *J. Geophys. Res.*, 101, 17547âĂŞ17559, doi:10.1029/96JB01508.

Cuffey, K., W. Patterson (2010), The Physics of Glaciers, *Elsevier*, 4th edn., Burlington, MA, USA

de Fleurian, O. Gagliardini, T. Zwinger, G. Durand, L. Le Meur, D. Mair, P. Råback (2014), A double continuum hydrological model for glacier applications *Cryosphere*, 8, 137-153, doi:10.5194/tc-8-137-2014.

Dow, C., A. Hubbard, A. Booth, S. Doyle, A. Gusmeroli, B. Kulessa (2013), Seismic evidence of mechanically weak sediments underlying Russel Glacier, West Greenland *Ann. Glac.*, 54, 135-141, doi:10.3189/2013AoG64A032.

Flowers, G., G. Clarke (2002), A multicomponent coupled model of glacier hydrology 1. Theory and synthetic examples *J. Geophys. Res.*, 107, 2287, doi:10.1029/2001JB001122.

Flowers, G. (2015), Modelling water flow under glaciers and ice sheets *Proc. R. Soc. London, Ser. A.*, 471, 2176, doi:10.1098/rspa.2014.0907.

Harper, Joel, N. Humphrey, T. Meierbachtol, J. Graly (2015),Characterization Of Greenland Ice Sheet Bed Conditions By Direct Measurement In A Network Of 36 Boreholes *Abstract C14A-04 presented at 2015 Fall Meeting*, AGU, San Francisco, CA, USA, 14-18 Dec.

Hewitt, I. J. (2011), Modelling distributed and channelized subglacial drainage: the spacing of channels, *J. Glaciol,*, 57, 302-314, doi:10.3189/002214311796405951.

Hewitt, I. J., C. Schoof, M. A. Werder (2012), Flotation and free surface flow in a model for subglacial drainage. Part 2. Channel flow, *J. Fluid. Mech.*, 702, 157-187, doi:10.1017/jfm.2012.166.

Hewitt, I. J. (2013), Seasonal changes i nice sheet motion due to melt water lubrication, *Earth Planet. Sci. Let.*, 371-371, 16-25, doi:10.1016/j.epsl.2013.04.022.

Hoffman, M., S. Price (2014), Feedbacks between coupled subglacial hydrology and glacier dynamics *J. Geophys. Res. Earth Surf.*, 119, 414-436. doi:10.1002/2013JF002943.

Meierbachtol, T., J. Harper, N. Humphrey (2013), Basal drainage system response to increasing surface melt on the Greenland ice sheet *Science*, 341, 777-779, doi:10.1126/science.1235905.

Nocedal, J., S. J. Wright (2006), Numerical Optimization, *Springer*, 2nd edn., New York, NY, USA

Rignot, E., P. Kanagaratnam (2006), Changes in the velocity structure of the Greenland ice sheet *Science*, 311, 986-990, doi:10.1126/science.1121381.

Ryser, C., M. Lüthi, L. Andrews, G. Catania, M. Funk. R. Hawley, M. Hoffman, F. Neumann (2014), Caterpillar-like ice motion in the ablation zone of the Greenland ice sheet *J. Geophys. Res. Earth Surf.*, 119, 2258-2271, doi:10.1002/2013JF003067.

Schoof, C. (2005), The effect of cavitation on glacier sliding *Proc. R. Soc. London, Ser. A*, 461, 609-627, doi:10.1098/rspa.2004.1350.

Schoof, C., I. J. Hewitt, and M. A. Werder (2012), Flotation and open water flow in a model for subglacial drainage. Part I: Linked cavities, *J. Fluid Mech.*, 702, 126âĂŞ156, doi:10.1017/jfm.2012.165.

SeaRISE website (2012), available at: `http://websrv.cs.umt.edu/isis/index.php/SeaRISE_Assessment`

Shepherd, A., A. Hubbard, P. Nienow, M. King, M. McMillan, I. Joughin (2009), Greenland ice sheet motion coupled with daily melting in late summer *Geophys. Res. Let.*, 36, 2-5, doi:10.1029/2008GL035758.

Sole, A., P. Nienow, I. Bartholomew, D. Mair, T. Cowton, A. Tedstone, M. King (2013), Winter motion mediates dynamic response of the Greenland ice Sheet to warmer summers *Geophys. Res. Let.*, 40, 3940-3944, doi:10.1002/grl.50764.

Sundal, A., A. Shepherd, P. Nienow, E. Hanna, S. Palmer, P. Huybrechts (2011), Melt-induced speed-up of Greenland ice sheet offset by efficient subglacial drainage *Nature*, 469, 521-524, doi:10.1038/nature09740.

Tsai, V., J. Rice (2010), A model for turbulent hydraulic fracture and application to crack propagation at glacier beds *J. Geophys. Res. Earth Surf.*, 115, 1-18. doi:10.1029/2009JF001474.

van de Wal, R. S. W., W. Boot, M. van den Broeke, C. Smeets, C. Reijmer, J. Donker, J. Oerlemans (2008), Large and rapid melt-induced velocity changes in the ablation zone of the Greenland Ice Sheet *Science*, 321, 111-113, doi:10.1126/science.1158540.

Werder, M., I. Hewitt, C. Schoof, G. E. Flowers (2013), Modeling channelized and distributed subglacial drainage in two dimensions, *J. Geophys. Res. Earth Surf.*, 118, 2140âĂŞ2158, doi:10.1002/jgrf.20146.

Wright, P., J. Harper, N. Humphrey, T. Meierbachtol (2016), Measured basal water pressure variability of the western Greenland Ice Sheet: Implications for hydraulic potential *J. Geophys. Res. Earth Surf.* , 121, doi:10.1002/2016JF003819.

Zwally, H., W. Abdalati, T.Herring, K. Larson, J. Saba, K. Steffen (2002), Surface-melt induced acceleration of Greenland Ice-Sheet flow *Science*, 297, 218-222, doi:10.1126.1072708.